Optica Applicata, Vol. XXXI, No. 2, 2001

Polarimetric optical fiber sensors for hydrostatic pressure and dynamic strain measurement

TOMASZ R. WOLIŃSKI, WITOLD KONOPKA, ANDRZEJ W. DOMAŃSKI

Faculty of Physics, Warsaw University of Technology, ul. Koszykowa 75, 00–662 Warszawa, Poland.

Polarization properties of the highly birefringent fibers and highly birefringent fiber-based polarimetric smart structure are discussed in view of potential applications to polarimetric optical fiber sensors for hydrostatic pressure and dynamic strain measurement.

1. Introduction

Fiber optic sensing systems are being presently tested in a variety of applications of smart structures and skins [1]–[4]. In particular, polarimetric sensors with highly birefringent (HB) polarization maintaining optical fibers have focused great interest for use in conjunction with composite materials. This growing interest has been mainly manifested in successful applications of HB fibers into fiber optic sensors based on polarimetric interference [4]. Influence of a variety of physical parameters on mode propagation in HB fibers is of special importance, since a number of physical quantities can be measured using the fibers. Recently, the suitability of HB few-mode fibers for the measurement of hydrostatic pressure, twist, and static and dynamic strain has been successfully demonstrated [4]–[10].

Much effort is being put forth at present to apply polarimetric fiber-optic sensors to measure strain in aircraft or concrete structures using the concept of so called smart skins and structures. In the last few years several researchers have published initial results of their investigations of polarimetric sensors structurally embedded in composite materials.

Smart structures and smart skin are structural components, particularly presumed for advanced aircrafts and space vehicles, with networks of fiber optic sensors directly embedded within their composite material matrices, which are valued by the aerospace industry for their light weight and high strength. The composite material is made with epoxies or polyimides. Structurally integrated polarimetric optical fiber sensors have emerged as an important part of sensors for smart structure applications. A more ambitious and complex use of smart structures involves linking fiber optic sensors with real-time computer-control system aboard advanced aircraft. In this model, fiber-optic sensors are embedded in a panel to be integrated with the wing. The sensors monitor environmental effects, such as strain and bending, around as well as within

the panel. In smart structures, fiber optic sensor becomes a part of the wing itself, and is of course not affected by electrical disturbance. In response to computer output, a fiber-optic link could drive remote actuators. A complete smart structure would not only detect problems but also respond to them instantaneously.

The paper briefly discusses polarization properties of the highly birefringent fiber-optic structures in view of potential applications to polarimetric optical fiber sensors for static and dynamic strain measurement. Selected experimental configurations were considered where both hydrostatic stress and dynamic strain were applied. Also mechanical properties of the epoxy structures have been investigated and the high sensitivity grating interferometry method [11] has been succesfully applied.

2. Polarization in optical fibers

In the description of polarization phenomena in optical fibers there are generally two approaches. The first one treats an optical fiber as an optical waveguide in which light being a kind of electromagnetic wave of optical frequencies can be guided in the form of waveguide modes. This approach identifies basic polarization eigenmodes of a fiber and relates them to the polarization state of the guided light. Changes in output polarization are described in terms of polarization-mode coupling due to birefringence changes acting as perturbations along the fiber.

Another approach treats an optical fiber like any other optical device which transmits light and the fiber can be divided into separated sections behaving like polarization state shifters. Here, polarization evolution in a fiber can be described by one of the three general formalisms: by the Jones vectors and matrices formalism, by the Stokes vectors and Mueller matrices formalism, or by Poincaré's sphere representation.

The magnitude of the internal birefringence (responsible for polarization phenomena) is characterized by the beat length of the two polarization modes

$$L_B = \frac{2\pi}{|\beta_y - \beta_x|} \tag{1}$$

and is responsible for phase difference changes along the longitudinal axis z of the HB fiber. The spatial period of these changes reflects the changes in the polarization states along the fiber. Since linearly birefringent fibers have a pair of preferred orthogonal axes of symmetry (birefringence axes), two orthogonal quasilinear polarized field components HE_{11}^{x} and HE_{11}^{y} of the fundamental mode HE_{11} (LP_{01}) which propagate for all values of frequency have electric fields that are polarized along one of these two birefringence axes. Hence, light polarized in a plane parallel to either axis will propagate without any change in its polarization but with different velocities. However, injection of any other input polarization excites both field components HE_{11}^{x} and HE_{11}^{y} and as these two orthogonal mode components are characterized by different

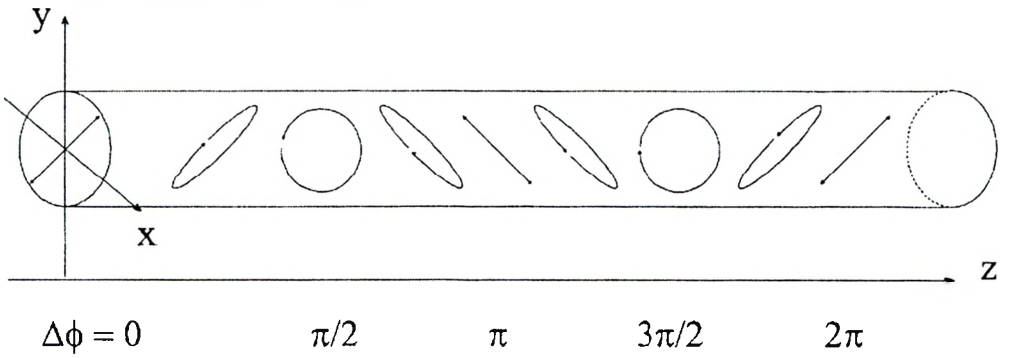

Fig. 1. Schematic representation of the beat length of the fundamental mode HE_{11} (LP_{01}) in HB fiber.

propagation constants β_x and β_y run into and out of phase at a rate determined by the birefringence of the HB fiber producing at the same time a periodic variation in the transmitted polarization state from linear through elliptic to circular and back again (Fig. 1).

3. Polarimetric fiber-optic sensors

Any symmetric deformation effect influences propagation constant β_i in every mode due to the changes in fiber length L and the refractive indices of the core and the cladding. This leads to changes in the phase $\Phi_i = \Delta\beta_i L$ along the fiber

$$\delta\Phi_i = \delta(\Delta\beta_i)L + \Delta\beta_i\delta L \tag{2}$$

where: $i = 0, 1, x, y$; $\delta\Phi_x, \delta\Phi_y$ are responsible for changes in the intensity distribution of light exciting the fiber under deformation and $\delta\Phi_0$, $\delta\Phi_1$ correspond to the output polarization state changes. The first case is the intermodal interference between X- or Y-polarized LP_{01} (HE_{11}) and LP_{11} spatial modes; whereas the second is in fact polarization interference between polarization modes LP_{01}^x and LP_{01}^y (or LP_{11}^x and LP_{11}^y) and requires use of an analyzer placed at the output of the fiber.

If the external perturbation is denoted by ξ, then an increase by $\delta\xi$ will cause the change in both $\Delta\beta_i$ and L by $\partial(\Delta\beta_i)/\partial\xi$ and $\partial L/\partial\xi$. So, from Eq. (2) one obtaines that

$$\delta\Phi_i = \left[\frac{\partial(\Delta\beta_i)}{\partial\xi}L + \Delta\beta_i\frac{\partial L}{\partial\xi}\right]\delta\xi = \frac{2\pi}{T_{i,\xi}}\delta\xi. \tag{3}$$

The quantities $T_{i,\xi}$ ($i = 0, 1, x, y$) have the dimension of the measurand ξ. These are experimentally measurable parameters and determine the sensitivity of the sensor to a given external perturbation.

In the fundamental LP_{01} (HE_{11}) mode the linearly polarized eigenmodes of HB fiber are associated with phase retardation ϕ_f and ϕ_s where subscripts f and s stand for

fast and slow azimuths, respectively. The total relative phase retardation between the two perpendicularly polarized eigenmodes propagating in HB fiber of a length L can be expressed as

$$\Delta\phi = \phi_f - \phi_s = \frac{2\pi}{\lambda}\Delta nL \tag{4}$$

where λ is the wavelength of the light and Δn equal to $n_f - n_s$, is the difference between the effective indices of the polarization modes. This phase retardation can be easily influenced by external factors (pressure, temperature, different stresses, *etc.*) and it creates the background of polarimetric fiber optic sensors. Two subcases, which are of great importance in the polarimetric fiber sensing applications, can be easily outlined: the single-mode polarimetric and the two-mode intermodal interferometric.

Single-mode regime of operation: the polarimetric sensor

This is the case were only one spatial mode LP_{01} or LP_{11} is excited at the input of a fiber. If the fiber is bimodal at the operating wavelength, single-mode regime can be achieved by adjusting the launching conditions. However, the practically popular solution is to use a single-mode optical fiber in which only the fundamental LP_{01} mode is propagating. No intermodal interference is observed in this case as the second mode is absent.

If quasimonochromatic light linearly polarized at an angle φ with respect to the X-axis of the fiber is launched into the fiber and an analyzer turned to an angle α is placed at the output of the fiber, then the optical intensity detected will be

$$I = \frac{1}{2}[1 + \cos 2\alpha \cos 2\varphi + |\gamma_0| \sin 2\alpha \sin 2\varphi \cos \Phi_0], \tag{5}$$

$\Phi_0 = \Delta\beta_0^0 L$ is the phase and γ_0 is a correlation function of the quasimonochromatic source. The same dependence is valid for the LP_{11}^x to LP_{11}^y polarimetric interference but $\Delta\beta_1^0$ should be substituted instead of $\Delta\beta_0^0$.

When external perturbations are introduced, they lead to changes in the phase $\Phi_0 = \Delta\beta_0^0 L$ of the fundamental LP_{01} mode. Consequently, it will lead to a cosine variation of the observed intensity I measured after the analyzer and that is in fact the polarization interference. The set-up is then a polarimetric sensor (Fig. 2). The interfering beams in this case are the LP_{01}^x and the LP_{01}^y polarization modes.
Visibility of the observed interference pattern defined as

$$V = \frac{I_{\max} - I_{\min}}{I_{\max} + I_{\min}} \tag{6}$$

is obtained to be

$$V = |\gamma_0| \frac{\sin 2\alpha \cos 2\varphi}{1 + \cos 2\alpha \cos 2\varphi}. \tag{7}$$

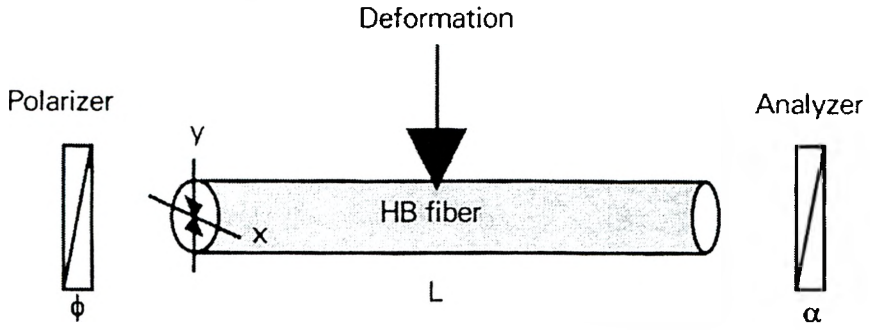

Fig. 2. Polarimetric configuration of a fiber-optic sensor – any deformation effect in an HB fiber modulates light intensity after the analyzer: $I(z = L) = 1/2[1 + \cos 2\alpha \cos 2\varphi + |\gamma_{/}| \sin\alpha \sin 2\varphi \cos\Delta\Phi_{/}]$, where $\Delta\Phi_{/}$ is the differential phase of the light leaving the HB fiber and $\gamma_{/}$ is a mutual correlation function.

The maximum visibility is obtained for $\varphi = \alpha = 45^{\circ}$. This is when both LP_{01}^{x} and LP_{01}^{y} polarization modes are equally excited by launching $\pm 45^{\circ}$ linearly polarized light. In this case, the observed intensity and the visibility become

$$I = \frac{1}{2}[1 + |\gamma_0| \cos(\Delta\beta_0^0 L)] \quad \text{with} \quad V = |\gamma_0| \tag{8}$$

If a monochromatic source is used, then visibility will become unit since $|\gamma_0| = 1$.

4. Experimental

The experimental set-up for optical response to hydrostatic pressure, which included a pig-tailed laser diode operated close to 633 nm wavelength, a fiber optic transducer, detection system and a pressure chamber, is presented in Fig. 3**a**.

The fiber-optic pressure transducer was connected to the pigtailed diode and detection system with FC/PC connectors. This makes the system more flexible and allows easy rearrangement. An IBM-PC with a specially designed interface built on the basis of advanced ADAM modules (Advantech Co., Ltd.) is used for data visualization. Pressure generation and calibration up to 300 MPa was performed by DWT pressure device. The proposed system is a step towards a commercial application of the smart structures based on polarization interferometry in fibers. The test samples were composed of the separated HB fibers, as well as the same HB fibers embedded in epoxy structures (Fig 4). The HB fiber-based samples and structures have been subjected to selected deformation effects mostly induced by hydrostatic pressure (up to 300 MPa) and temperature, whereas polarization properties of the transmitted optical signal have been investigated.

The lead-in and lead-out fibers were composed of Fibercore bow-tie HB waveguides. For some experiments sensing samples composed of different types of bow-tie and side-hole HB fibers embedded in an epoxy structure (of 7 mm in diameter, and 110 mm in length, Fig 4) were investigated. To create the structures the

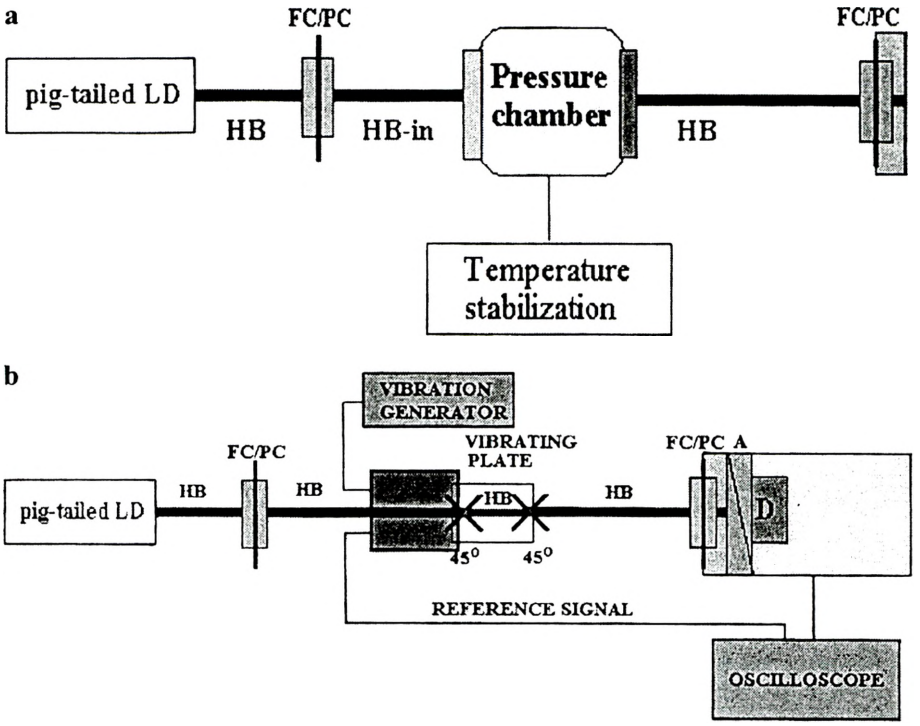

Fig. 3. Experimental set-up for the static (**a**) and dynamic (**b**) measurements; fiber optic transducer is connected to a PC by the interface ADAM–4017 (FC/PC – optical connectors, D – detector).

EPIDIAN-5 epoxy glue (Young's modulus $E = 1273.13$ N/mm^2) was used. Due to the precise fiber splicer Ericsson FSU 925 PM and angle between the sensing structures and lead-in or lead-out fibers birefringence axes could be chosen arbitrarily. A few configurations were investigated: with the angles of 10°, 20°, 30°, and 45°.

A different set-up had to be applied in order to measure the optical response of the fiber optic sensor to a dynamic strain. The set-up included a pig-tailed laser diode at 633 nm wavelength, fiber optic transducer, detection system and vibrating plate, see Fig. 3**b**. The HB transducer, also presented in Fig. 3**b** is glued on to the vibrating piezoceramic plate. The plate is, in fact, composed of two plates, glued together, one generating vibrations (connected with the vibration generator) and the other monitoring vibrations connected to the oscilloscope. The output optical signal is collected at the detector after passing through the analyzer which is set along the fiber axis. Such a set-up enables calibration of the dynamic sensor based on the HB fiber.

In order to investigate the mechanical response of the structure to the external load applied a grating interferometry method was used. A laboratory grating interferometer is presented in Fig. 5. The He-Ne laser beam is filtered, expanded and collimated. The two illuminating beams have been obtained by the system of three mirrors M1, M2 and M3, attached rigidly to the specimen. The grating is glued to face of the sample (smart structure) and axially loaded (Fig. 5) along the Y-axis. As a result of the

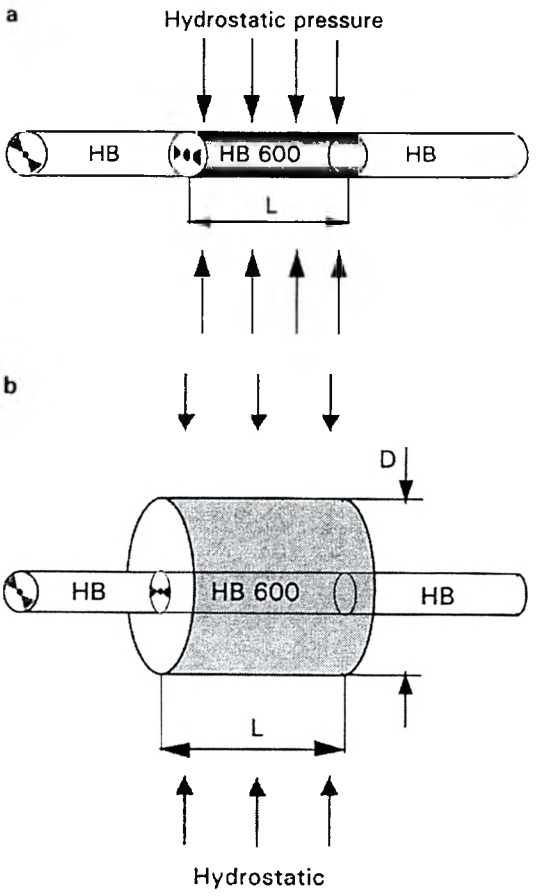

Fig. 4. Separated HB sensing fiber (**a**) and the HB fiber embedded in the cylindrical epoxy structure (**b**). The lead-in and lead-out HB fibers could be spliced at different angles.

interference of beams A and B, the fringe pattern representing $u(x,y)$ in-plane displacements is created, while the beams C and D give the information about the $v(x,y)$ displacements. The specimen grating SG is imaged with the proper magnification in the CCD detector matrix plane. The interference pattern obtained is grabbed with the Frame Grabber and then processed with the fringe application program [11].

The intensity distribution in the image plane can be described by equation

$$I \propto a_0 + b_1 \cos\frac{4\pi}{d}[u(x,y)] + b_2 \cos\frac{4\pi}{d}[v(x,y)] \tag{9}$$

where: a_0 – background, b_1, b_2 – local contrast, d – diffraction grating period, λ – wavelength, $u\ (x, y)$ and $v\ (x, y)$ – in-plane displacement functions.

However, such a set up allows only one of the displacement components (*i.e.*, $u\ (x, y)$ or $v\ (x, y)$) to be measured at a time. Thus, either b_1 or b_2 is equal to 0 at the time of the measurement.

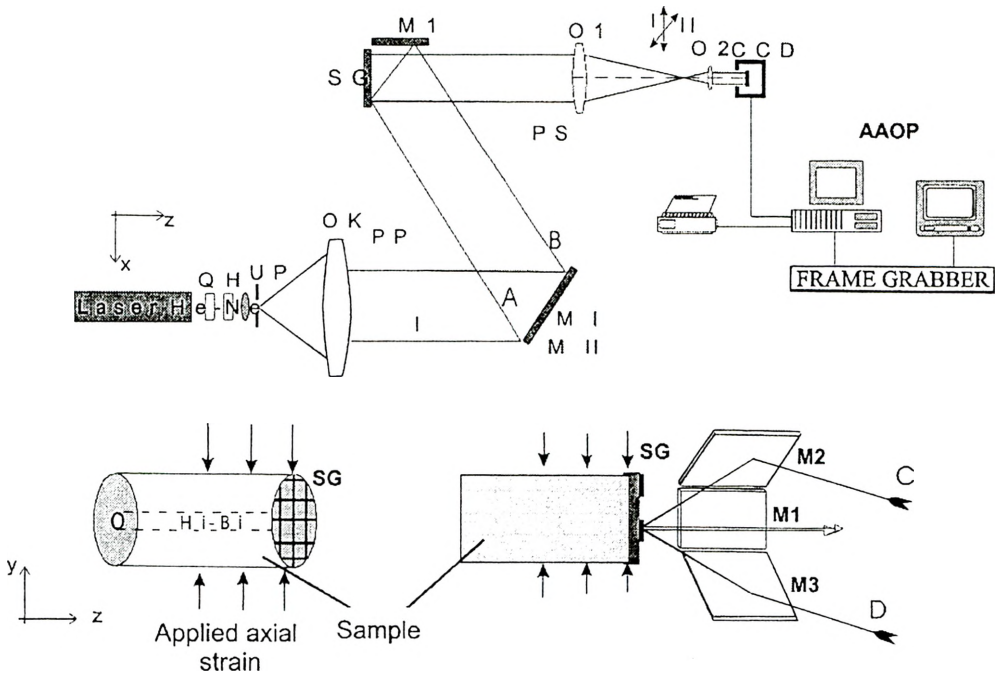

Fig. 5. Experimental set-up: I – $v(x,y)$ plane, II – $u(x,y)$ plane, SG – specimen grating, A, B, C, D – parts on illuminating beam, M – mirror, O1, O2 – imaging objectives with magnification ~ 1 or 3, M1, M2, M3 – mirrors of the interferometer head, OK – collimating objective, UP – pinhole system.

5. Results

It appears that the presence of the epoxy coating modifies the output characteristics of the HB fiber (mostly due to elastic properties of the structure) as well as the level of the induced birefringence of the HB fiber, and hence, influences polarization properties of the light propagating in the fiber.

However, for the sensor embedded in the structure one can observe a change in the period of its sine-like characteristics. The hydrostatic pressure characteristic of smart structures has a fundamental period T_p ~100 MPa, which is twice as large as the period of the separated fibercore HB-600 bow-tie fiber (T_p ~50 MPa), see Fig. 6**a**. Hence, the presence of the epoxy structure significantly modifies the output characteristics of the HB fiber. As a consequence, the induced birefringence of the embedded HB fiber changes less drastically than for the separated HB fiber probably due to the fact that pressure induced stresses in the structure are separated between both the epoxy coating and the embedded HB fiber. A comparison of the polarimetric HB fiber and the HB structure parameters is presented in Tab. 1.

The optical response of different polarimetric fiber optic sensors under various external factors always shows sine-like behaviour. Furthermore, some conclusions about the smart structures themselves can be drawn from Fig. 6**b**. The period T_p that

is an amount of pressure required to induce 2π phase shift between both polarisation components of the fundamental mode does not depend on the angle between the birefringence axes of the sensing structures and lead-in fibers. Nevertheless, an amplitude of changes of the output signal (modulation depth) varies significantly with this angle. In Table 2, different samples of smart structures are compared.

Under hydrostatic pressure the birefringence of the HB-600 fiber changes according to the formula

$$\Delta\beta = \Delta\beta_0\left(1 + \frac{pL_{B_0}}{LT_p}\right) \tag{10}$$

where $\Delta\beta_0$ signifies the modal birefringence without external pressure, L_{B_0} is a beat-length value at ambient temperature and without external pressure, p is a pressure,

Table 1. Comparison of parameters of the polarimetric HB fiber and HB fiber-based polarimetric structures.

Parameters	HB fiber	HB structure	HB structure 2
Angle between axes [deg]	45	45	30
Length of the sensor L [mm]	12	12	12
Diameter Φ [mm]	0	7	7
Period T_p [MPa]	50	100	100
Sensivity $\eta = 2\pi/T_p$ [1/MPa]	0.126	0.0628	0.0628
Sensivity per unit length $S = 2\pi/L \times T_p$ [1/m×MPa]	10.5	5.2	5.2

Table 2. Comparison of an optical response of HB fiber-based polarimetric smart structures at different input polarization angles.

	HB fiber-based polarimetric smart structures			
Angle between axes [deg]	45	30	20	10
Length of the sensor L [mm]	12	12	12	12
Diameter Φ [mm]	7	7	7	7
Modulation depth (max/min)	12	9	4	2
Pressure-sensitivity expressed as $\alpha_p = (1/I)\, dI/dp$ calculated in the linear region of pressure characteristics	5×10^{-2}	4.8×10^{-2}	3.34×10^{-2}	1.67×10^{-2}

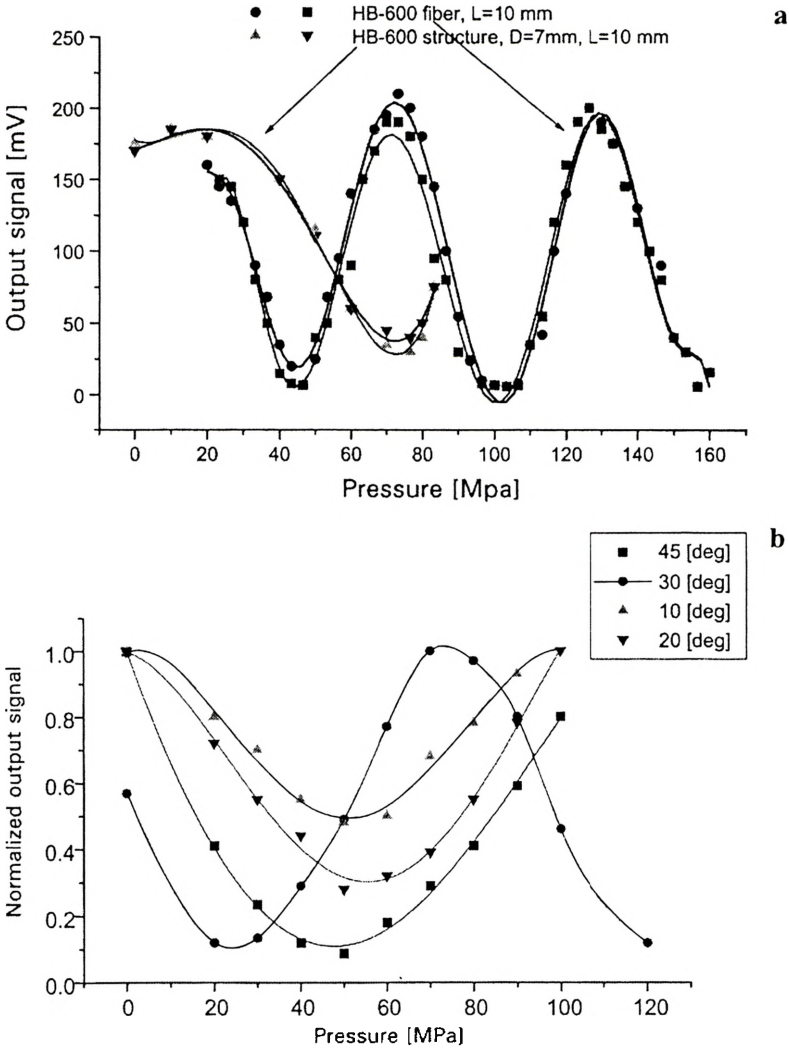

Fig. 6. Comparision of the pressure characteristics of the separated HB fiber and the HB fiber-based polarimetric smart structure (Fibercore bow-tie HB-600 fiber) (**a**), optical responses of the smart structures (12 mm in length) under hydrostatic pressure at various input polarization angles (Fibercore bow-tie HB-600 fiber) (**b**).

L stands for the length of the fiber, and T_p is an amount of pressure required to induce 2π phase shift between both polarization components of the fundamental mode [10]. A comparison of the changes in birefringence of the separated HB fiber and embedded in structure as a function of hydrostatic pressure is shown in Fig. 7, along with some data calculated for PANDA HB fiber.

The characteristic of bow-tie smart structures under hydrostatic stress presented in Fig. 6**a** has a fundamental period T_p~100 MPa, which is 20 times larger than the period

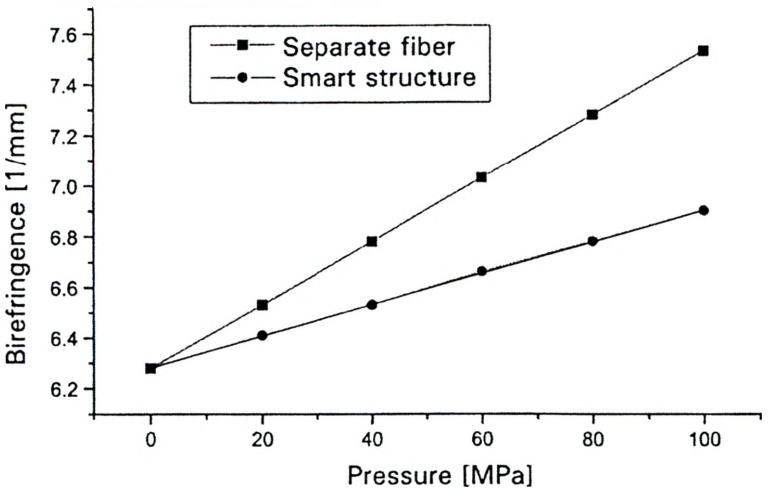

Fig. 7. Birefringence responses of the separated HB bow-tie fiber and the fiber embedded in structure at various values of hydrostatic pressure.

of Maria Curie-Skłodowska University (UMCS), Lublin, Poland, side-hole smart structure characteristics, Fig. 8, Tab. 3. This means that smart structure based on UMCS side-hole HB fibers shows much better sensitivity. It should also be noted that in contrast to smart structures based on bow-tie fibers, for smart structures with side-hole fiber a good thermal stability was observed. The reason for that is that pressure and thermal sensitivity of the bow-tie fiber are of the same order, whereas pressure sensitivity of the side-hole fiber is two orders of magnitude higher than its temperature sensitivity [12].

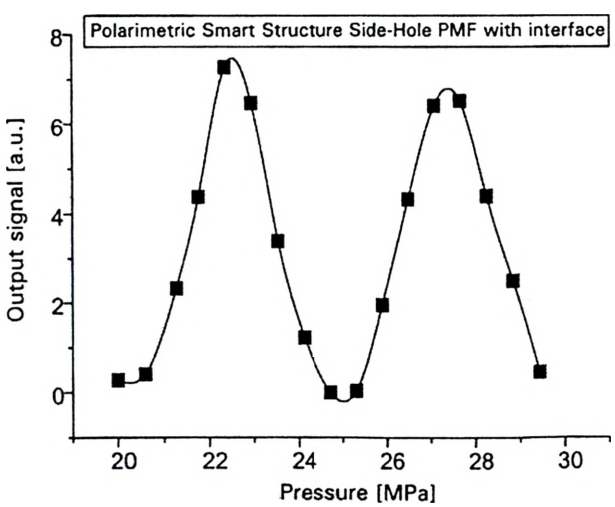

Fig. 8. Optical response of the HB side-hole (UMCS, cat. no. V) fiber-based polarimetric smart structure to hydrostatic pressure.

Table 3. Comparison of the HB fiber-based polarimetric smart structures with fibercore bow-tie and UMCS side-hole HB fibers.

Parameters	Smart structures with Fibercolor bow-tie	Smart structures with UMCS side-hole
Length of the sensor L [mm]	12	12
Diameter Φ [mm]	7	7
Period T_p [MPa]	100	5
Sensitivity $\eta = 2\pi/T_p$ [1/MPa]	0.0628	1.256
Sensitivity per unit length $S = 2\pi/L \times T_p$ [1/m×MPa]	5.2	104.6
Pressure-sensitivity expressed as $\alpha_p = (1/I)\, dI/dp$ calculated in the linear region of pressure characteristics	5×10^{-2}	5.3×10^{-1}

Hence, the presence of the epoxy structure significantly modifies output characteristics of the HB fiber. As a consequence, birefringence of the embedded HB fiber changes less drastically than for a separated HB fiber, probably due to the fact that pressure induced stresses in the structure are distributed in both epoxy structure and the HB fiber (clad and core regions). This means that the epoxy cylinder isolates (to some extent) the birefringent fiber from the external load. We expected that this could be explained using the results of the measurements of displacements occurring in the structure under axial load.

In Figure 9**a**, results of measurement of the $v(x,y)$ displacements in the whole sample are presented. One can notice that the displacement has the highest value at the edge of the smart structure where the forces are applied and it linearly changes along the sample. However, since the fiber diameter is very small in comparison with the diameter of the whole sample the effects occurring just next to the fiber can hardly be observed in pictures showing the whole structure. Thus we also performed the measurement with the applied optical zoom in order to find out the mechanical response of the structure in the area next to the fiber, see Fig. 9**b**. It turned out that next to the fiber the displacement is no longer linear and the displacement gradient changes its sign, which is probably due to difference of Young's modulus of the epoxy glue and the glass. All this confirms what we suspected, that epoxy cylinder isolates the fiber from the external loads.

Yet another observation was made during the measurements with the grating interferometry method, that there was no plastic stain after the measurements.

As regards the experiment in which the dynamic strain was measured, the output from the oscilloscope is presented in Fig. 10. The upper characteristic is the reference signal generated by the monitoring plate. The lower one is the optical output. Since

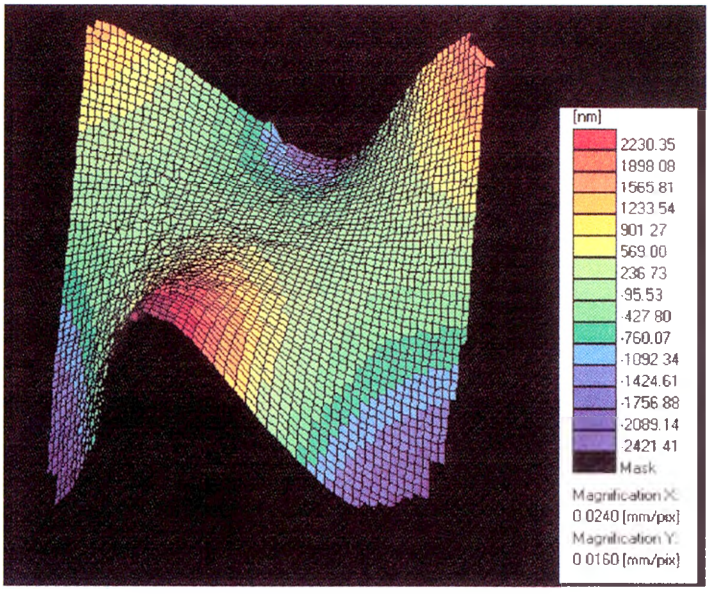

a

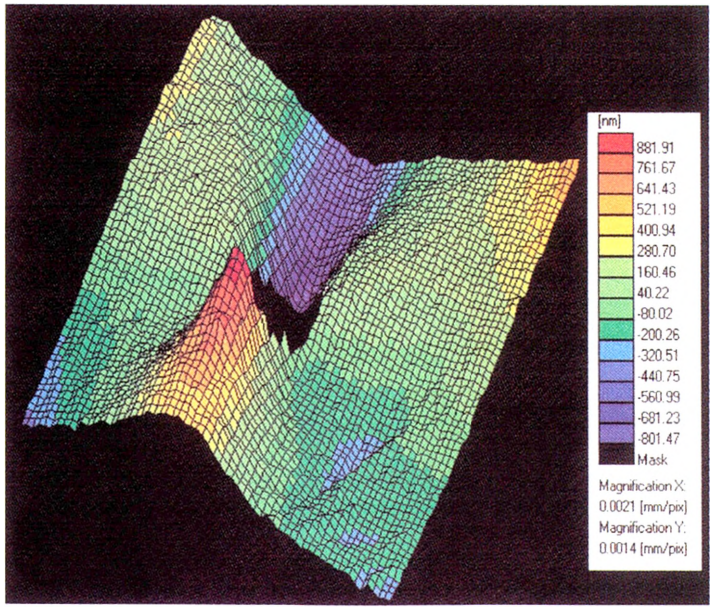

b

Fig. 9. 3-D plot of the $v(x,y)$ displacements in the whole structure under axial load in two fields of view: 5×5mm (a) and 1×1mm (b).

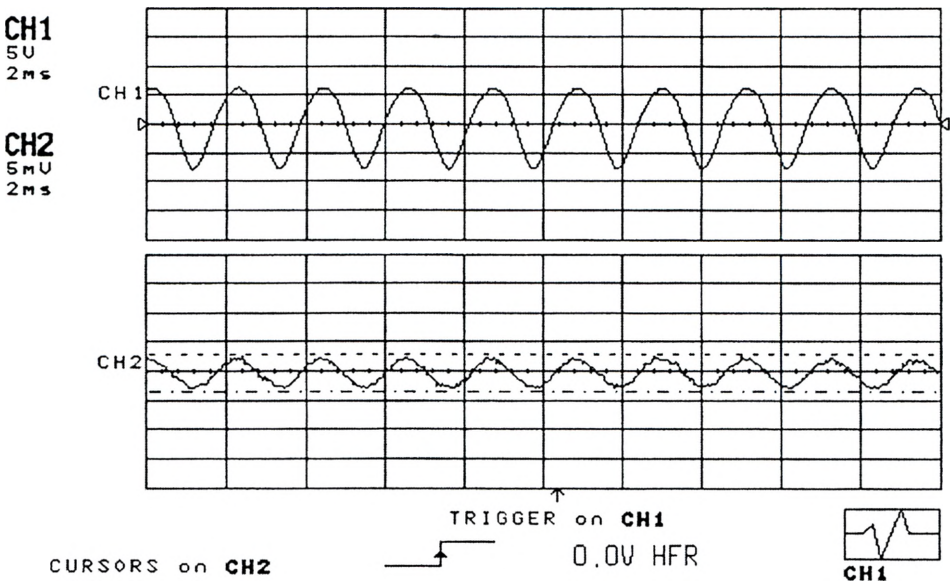

Fig. 10. Output of the LeCroy LS140 oscilloscope comparing dynamic strain measurement with piezoceramic (CH1) and HB fiber-based optical (CH2) sensor.

the calibration curve of the monitoring plate was supplied by the producer, this enabled us to determine the displacement in mm and create the calibration curve for the HB fiber-based optical dynamic sensor.

6. Conclusions

We have demonstrated that the fiber optic polarimetric sensors are suitable for measurements of both static and dynamic external loads. The dynamic sensor was calibrated with a device using a vibrating piezoceramic plate.

Both the optical and mechanical experiments have shown that the epoxy structure isolates the fiber from the external load, but it does not change the shape of optical response of the fiber optic polarimetric sensors.

The smart structure composed of UMCS side-hole fiber shows much better sensitivity than that composed of Fibercore HB-600 bow-tie fiber. Thus, the bow-tie fiber embedded in an epoxy container is suitable for pressure sensing application up to 300 MPa, whereas side-hole smart structure is more suitable for smaller ranges but with higher accuracy. The observed thermal stability of side-hole smart structures makes them very promising for commercial applications.

Acknowledgments – The work was partially supported by the Photonics Engineering Research Project of the Warsaw University of Technology and by the Polish State Committee for Scientific Research (KBN) under the grant no. 8 T11D 01218. The authors are grateful to Dr. J. Wójcik (UMCS, Lublin) for fruitful collaboration. The support of Ericsson Company is also gratefully acknowledged.

References

[1] UDD E., *Fiber Optic Sensors*, Willey, New York 1991.
[2] WOLIŃSKI T. R., DOMAŃSKI A. W., GAŁĄZKA P., *Multiplexed Polarimetric Sensors with Highly Birefringent Optical Fibers for Smart Structures*, [In] *Polarimetry and Ellipsometry*, Proc. SPIE **3094** (1997), 218.
[3] CALERO J., SOU-PAN WU, POPE C., *et al.*, J. Lightwave Technol. **12** (1994), 1081.
[4] WOLIŃSKI T. R., *Polarimetric optical fibers and sensors*, [In] *Progress in Optics*, [Ed.] E. Wolf, Vol. XL (2000), 1–75, Elsevier Science B.V., North Holland.
[5] BOCK W. J., DOMAŃSKI A. W., WOLIŃSKI T. R., Appl. Opt. **29** (1990) 3484.
[6] BOCK W. J., WOLIŃSKI T. R., EFTIMOV T., Pure and Applied Optics: J. Europ. Opt. Soc. **5** (1996), 125.
[7] WOLIŃSKI T. R., KONOPKA W., DOMAŃSKI A. W., *Polarization interferometry in fiber optic smart structures*, [In] *Laser Interferometry IX: Techniques and Analysis*, Proc. SPIE **3478**, (1998), 421.
[8] KONOPKA W., WOLIŃSKI T. R., DOMAŃSKI A. W., *Polarization properties of smart structures based on highly birefringent fibers*, [In] *Interferometry '99: Applications*, Proc. SPIE **3745** (1999), 319.
[9] WOLIŃSKI T. R., KONOPKA W., DOMAŃSKI A. W., *Polarization-based fiber-optic smart structures*, [In] *Polarisation and Colour Techniques in Industrial Inspection*, Proc. SPIE **3826** (1999) 264.
[10] BOCK W. J., WOLIŃSKI T. R., BARWICZ A., IEEE Trans. Instrum. Meas. **39** (1990), 715.
[11] KUJAWIŃSKA M., SAŁBUT L., Opt. Appl. **25** (1995), 211.
[12] WÓJCIK J., JANOSZCZYK B., MERGO P., *et al.*, *Prototype HB side-hole fiber*, V Conf. Appl. Optical Fibers, Białowieża, Poland, January 22–24, 1998, pp. 301–308.

Received October 30, 2000
in revised form June 12, 2001